

Berezinskii - Kosterlitz - Thouless transition in rhenium nitride films

Kosuke Takiguchi,* Yoshiharu Krockenberger, Yoshitaka Taniyasu, and Hideki Yamamoto
NTT Basic Research Laboratories, NTT Corporation,
3-1 Morinosato-Wakamiya, Atsugi, Kanagawa 243-0198, Japan
 (Dated: January 24, 2024)

The quest to manipulate and understand superconductivity demands exploring diverse materials and unconventional behaviors. Here, we investigate the BKT transition in synthesized ReN_x thin films, demonstrating their emergence as a compelling platform for studying this pivotal phenomenon. By systematically varying synthesis parameters, we achieve ReN_x films exhibiting a BKT transition comparable or even surpassing the archetypal NbN_x system. Detailed current-voltage measurements unlock the intrinsic parameters of the BKT transition, revealing the critical role of suppressed superconducting volume in pushing ReN_x towards the two-dimensional limit. Utilizing this two-dimensional electron system, we employ Beasley-Mooij-Orlando (BMO) theory to extract the vortex unbinding transition temperature and superelectron density at the critical point. Further confirmation of the BKT transition is obtained through temperature-dependent resistivity, current-voltage, and magnetoresistance measurements. Our findings suggest that native disorder and inhomogeneity within ReN_x thin films act to suppress long-range coherence, ultimately driving the system towards the BKT regime. This work establishes ReN_x as a promising material for exploring BKT physics and paves the way for tailoring its properties for potential applications in superconducting devices.

I. INTRODUCTION

The pursuit of understanding and manipulating superconductivity continues to drive innovation across physics and material science. In this realm, superconducting thin films offer fertile ground for exploring diverse phenomena due to their controllable geometry and sensitivity to external factors. Among these, the Berezinskii-Kosterlitz-Thouless (BKT) transition [1–3] holds a unique position, unveiling the interplay between order and disorder within the vortex condensate.

In essence, the BKT transition marks a crucial shift from a state with quasi-long-range order in the vortex world to a fully disordered regime as temperature increases. This transition, originally conceptualized for two-dimensional (2D) systems, finds profound relevance in thin films where finite thickness creates an effective 2D superconducting layer. Studying the BKT transition in these systems unlocks valuable insights into fundamental aspects of vortex dynamics, phase fluctuations, and the interplay between dimensionality and superconductivity.

The importance of the BKT transition stems from its multifaceted influence on superconducting properties. Its influence extends beyond a simple phase change, impacting a variety of observable characteristics. Regarding electronic transport, the characteristic discontinuities in resistivity near the BKT temperature T_{BKT} unveil the breakdown of phase coherence and the emergence of dissipative processes. The magnetization behavior of the BKT transition leaves its footprint in the hysteresis behavior of magnetization, reflecting the collective dynamics of unbound vortices. Furthermore, the BKT transition plays a pivotal role in understanding the interplay

between superconductivity and other phase transitions, particularly the superconductor-to-insulator transition. By tuning film thickness, disorder, and external fields, researchers can manipulate the BKT transition and explore this intriguing interplay, paving the way for novel device functionalities [4–11].

In light of these multifaceted implications, a meticulous investigation of the BKT transition in superconducting thin films remains an active and impactful area of research. This manuscript delves into the intricacies of this fascinating phenomenon, shedding light on its mechanisms, consequences, and potential applications. Through detailed analysis of experimental data and theoretical frameworks, we aim to deepen our understanding and pave the way for further exploration of this remarkable transition in the fascinating world of superconducting thin films.

For this purpose, the choice of the experimental platform is crucial. Homogeneously disordered superconducting thin film materials are widely studied for the BKT physics though a clear distinction between three-dimensional superconductivity and 2D BKT transitions appears to be challenging. In fact, truly long-range homogeneously disordered thin film materials without superconducting domains are a major issue for experimental characterization of the BKT transition. The NbN_x system is a favorite to investigate the BKT phase transition. Yet, several shortcomings associated to it need to be addressed. One of the major issues is that NbN_x can be synthesized with long-range crystalline coherence using standard synthesis techniques such as radio frequency (RF) sputter [12]. As such long-range coherence of crystalline phases is not desirable for the investigation of the BKT transition, the films have to be extremely thin ($< 3 \text{ nm}$) [4–8] or subject to Ar ion bombardment [9]. After subjecting NbN_x to Ar ion plasma, NbN_x may

* kosuke.takiguchi@ntt.com

partially dissociate, leaving Nb instead. However, Nb is a superconductor by itself with a superconducting transition temperature nearby that of NbN_x . Similar experimental requirements have been reported also for TiN films [10].

Here, we introduce the ReN_x system as an alternative materials system for the investigation of the BKT transition. Compared with the NbN_x and the TiN system, the ReN_x system is not in favor of long-range crystallographic coherence and high-pressure-high-temperature synthesis techniques are required. Such a thermodynamic behavior is beneficial for the investigation of the BKT transition as the as-grown material is sufficient to mimic a large-scale Josephson junction system [13]. In the ReN_x system, superconducting (ReN [14, 15] and ReN_2 [16]) and non-superconducting phases (Re_3N [17], Re_7N_3 [18], Re_2N [17], Re_3N_2 [19], ReN_3 [19], ReN_4 [19] and ReN_{10} [19]) are known. The variety of ReN_x phases reported originates from the covalent bonding character of Re and N [19]. In contrast, for NbN - a $4d$ nitride system - the ionic character increases. Notably, ionic character for TiN - a $3d$ system - appears to be highest. As the ReN_x system easily enables coexisting superconducting and non-superconducting phases, introduction of the necessary disorder appears to be easier than in the NbN_x system.

In this paper, we report the BKT transition in ReN_x films. Magnetization measurements using a superconducting quantum interference device (SQUID) on ReN_x films show a transition from fully diamagnetic thin films towards ReN_x films with a paramagnetic response. Using the theory of Beasley, Mooij, and Orlando (BMO)[20], we confirm the BKT transition by temperature dependence of resistivity, non-linear current-voltage characteristics, and magnetoresistance data even in the sample with the smallest superconducting volume. Our results on the BKT behavior of the ReN_x system show that it can be considered as an alternative model system for the investigation of the BKT transition.

II. EXPERIMENTAL DETAILS

ReN_x thin films were synthesized on $\text{KTaO}_3(001)$ substrates by molecular beam epitaxy. We synthesized five samples: (I) 7.8-nm-thick ReN_x grown at $T_s = 500^\circ\text{C}$, (II) 7.8-nm-thick ReN_x grown at 600°C , (III) 7.8-nm-thick ReN_x grown at 700°C , (IV) 19.5-nm-thick ReN_x with 1.5 mol % praseodymium (Pr) grown at $T_s = 700^\circ\text{C}$, and (V) 39-nm-thick ReN_x with 1.5 mol % Pr grown at $T_s = 700^\circ\text{C}$. T_s represents the growth temperature. A custom-designed nitrogen RF source is used for the nitrification of Re with a typical N_2 flow rate f_{N_2} of 2.0 sccm. The RF radical power $P_{\text{RF}} = 400\text{ W}$ in samples I-III, and 350 W in samples IV and V. Detailed information of the sample growth and structure determination are given in [21]. Re_2N is a non-superconducting phase in the ReN_x system and the synthesis conditions

used determine the ratio between superconducting ReN and non-superconducting Re_2N [17]. Higher synthesis temperatures favor the formation of ReN . If very high synthesis temperatures are required, the introduction of a catalyst appears to be beneficial. It is desired that the catalysts electronic behavior is insulating and we therefore deposited praseodymium [22, 23]. Under flowing atomic nitrogen, rare earth elements readily form rare earth nitrides, which are electronically insulating [24]. Addition of Pr enables an additional control parameter of the superconducting volume fraction associated with ReN .

Samples I-IV were used for transport and magnetization measurements. Additional data taken of sample III and V are shown in [21]. Resistivity (ρ) measurements were performed using a standard four-probe method with 40 nm silver electrodes. Temperature dependence of ρ , electrical current-voltage ($V(I)$) characteristics, and magnetoresistivity were measured in a Quantum Design Dynacool PPMS under magnetic fields applied perpendicular to the film surface. Electronic transport measurements between 100 mK and 1.8 K are carried out using a ^3He - ^4He dilution refrigerator option on Quantum design PPMS.

III. RESULTS AND DISCUSSION

A. Temperature dependence of magnetic moment

Figures 1(a-c) show the temperature dependence of magnetic moment for samples I, II, and IV. An external magnetic field of $H = 10\text{ Oe}$ was applied in the in-plane direction of the film. For sample I [Fig. 1(a)], one can see the transition to the positive magnetic signal below $T_{c0} = 3.53\text{ K}$ in both field cooling (FC) and zero field cooling (ZFC). T_{c0} represents the mean field critical temperature. Since the formation of Cooper pairs is hindered due to the inhomogeneity, superelectrons yields a paramagnetic signal in the temperature range of the BKT phase. In the previous reports, the positive magnetic response is typical in a Josephson-junction array or superconducting thin films in the two-dimensional limit [25]. The positive response in FC is larger than that in ZFC, and this is a different feature of Meissner effect in superconductors. In sample II, this behavior is also observed at $T_{c0} = 4.00\text{ K}$, and the moment below T_{c0} is suppressed rather than that of sample I. The diamagnetic signal becomes greater than the positive signal from the BKT state below $T_{di} = 3.10\text{ K}$. T_{di} is temperature below which the magnetic moment decreases in ZFC. The inflection points in FC coincides with T_{di} , implying that the transitions seen in FC and ZFC occur from the same origin. The coherency between superelectrons develops below T_{di} . The situation, in which the diamagnetic signal overcomes the positive magnetic response by BKT state, is more pronounced in sample IV. Meissner effect is clearly seen in FC and ZFC, respectively. When

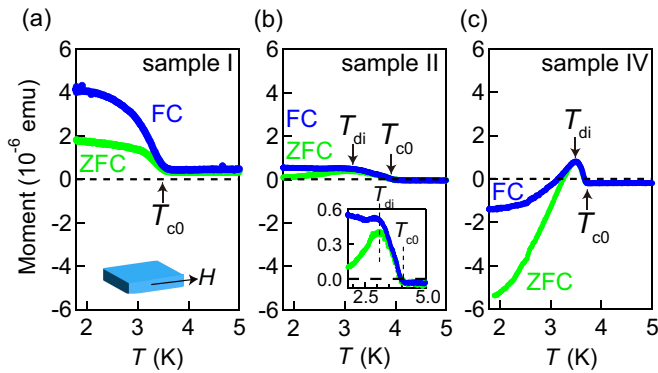


FIG. 1. Temperature dependence of magnetic moment of samples (a) I (b) II, and (c) IV. The applied magnetic field of $H = 10$ Oe is parallel to the in-plane direction of the film. For each sample shown here, field-cooled (FC) and zero field cooled (ZFC) measurement data are plotted. The inset of (b), a magnified view of the magnetization in the vicinity of T_{di} and T_{c0} is plotted. The dashed line indicates the zero moment. Note that the magnetization remains positive at all temperatures for samples I and II. On the other hand, shielding (ZFC) and Meissner (FC) diamagnetic signals are clearly observed in (c).

$3.48 \text{ K} (= T_{di}) < T < 3.70 \text{ K} (= T_{c0})$, the positive magnetic response is observed as well as in samples I and II. On the other hand, below T_{di} , Meissner effect dominates the temperature dependence of the moment due to the large superconducting volume. We confirmed this by doubling the thickness of ReN_x (sample V, see [21]), and x-ray diffraction data confirm the existence of ReN_x with $x \simeq 1$. In contrast, large crystalline volumes are not seen for other samples discussed here.

B. Temperature dependence of resistivity

Next, we show temperature dependence of resistivity (ρ) [Fig. 2(a-c)] of samples I, II, and IV, respectively. The normal state resistivity at 5.0 K ρ_N are shown in Table I. From ρ_N , we can discuss the inhomogeneity of our ReN_x by employing the NbN data in the previous report since NbN has the same crystal structure of ReN. Using a Fermi velocity $v_{F,\text{NbN}} = 1.52 \times 10^6 \text{ m/s}$ and carrier concentration $n_{\text{NbN}} = 7.60 \times 10^{28} \text{ m}^{-3}$ equal to what have been reported for NbN [12], the BCS coherence length $\xi_0 (= 0.18 \hbar v_{F,\text{NbN}} / k_B T_{c0})$ and the mean free path $\ell (= m v_{F,\text{NbN}} / e^2 \rho_N n_{\text{NbN}})$ are also calculated (Table I), where k_B is Boltzmann constant, m is electron mass, and e is elementary charge. ℓ becomes longer in the order of samples I, II, and IV as the crystallized volume increases. All ℓ in samples I, II, and IV are shorter than 0.3% of ξ_0 . Hence, the dirty limit condition is fulfilled ($\ell \ll \xi_0$), and the disordered state for the BKT phenomenon is realized. Near T_{BKT} , spontaneous creation and annihilation of vortex-antivortex pairs terminates long-range coherency and zero resistance emerges

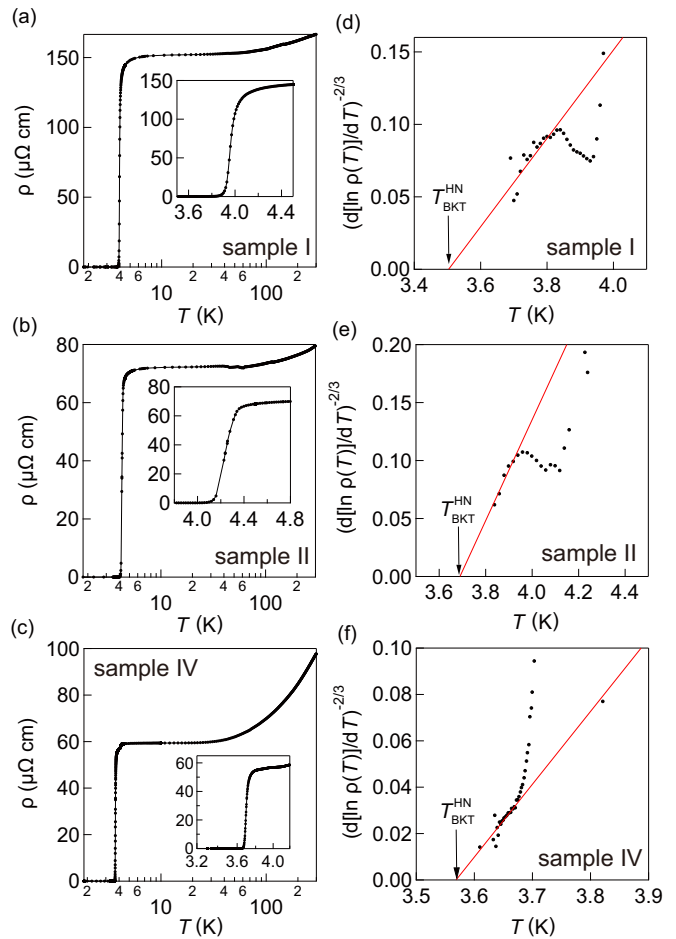


FIG. 2. In Figs. (a), (b), and (c), the resistivity of samples I, II, and IV are plotted as a function of temperature (logarithmic scale). The insets in (a)-(c) enlarge on the resistivity drop to $\rho = 0$ around T_{di} . Note that the temperature is plotted linearly. In (d)-(f), we plot $(d \ln \rho(T) / dT)^{-2/3}$ as a function of temperature for ρ in the vicinity of T_{di} . The straight fitting curve intercepts $(d \ln \rho(T) / dT)^{-2/3} = 0$ to reveal $T_{\text{BKT}}^{\text{HN}}$.

at temperatures where fluctuations are sufficiently suppressed. This transition corresponds to the BKT transition. According to the theory of Halperin-Nelson [26] on the BKT transition, the $\rho(T)$ behavior in this region follows

$$T - T_{\text{BKT}} \propto \left(\frac{d \ln \rho(T)}{dT} \right)^{-\frac{2}{3}}. \quad (1)$$

As shown in Fig. 2(d-f), we fitted the $\rho(T)$ data using Eq. (1). The fitting intervals of samples I, II, and IV are $3.70 \text{ K} < T < 3.84 \text{ K}$, $3.84 \text{ K} < T < 3.94 \text{ K}$, and $3.61 \text{ K} < T < 3.67 \text{ K}$, respectively. The estimated transition temperature ($T_{\text{BKT}}^{\text{HN}}$) and superfluid stiffness $J_s = 2T_{\text{BKT}}^{\text{HN}} / \pi$ are shown in Table II. According to the BMO theory [20], the relation between T_{BKT} and the

TABLE I. Growth condition, electronic transport parameters and magnetization parameters determined for samples I, II, and IV. ρ_N is the resistivity obtained at 5.0 K in each sample.

Sample	T_s (°C)	Pr (%)	f_{N_2} (sccm)	P_{RF} (W)	T_{c0} (K)	ξ_0 (nm)	ρ_N ($\mu\Omega$ cm)	ℓ (nm)	$\mu_0 H_{c2}(0)$ (T)	$\xi_{GL}(0)$ (nm)
I	500	0	2.0	400	3.54	590	152 ± 9.83	0.47 ± 0.03	3.55 ± 0.008	9.63 ± 0.01
II	600	0	2.0	400	4.00	522	72.7 ± 4.69	0.98 ± 0.06	3.83 ± 0.014	9.27 ± 0.02
IV	700	1.5	2.0	350	3.70	565	39.4 ± 1.06	1.80 ± 0.05	1.51 ± 0.004	14.8 ± 0.02

TABLE II. BKT parameters determined for samples I, II, and IV. J_s , n_s^{2D} , and λ_\perp were estimated by using T_{BKT}^{HN} according to $J_s = 2T_{BKT}^{HN}/\pi$, Eq. (2), and Eq. (3), respectively.

Sample	T_{BKT}^{HN} (K)	T_{BKT}^α (K)	J_s (K)	n_s^{2D} (10^{15} m $^{-2}$)	λ_\perp (nm)
I	3.50 ± 0.48	3.46	2.23 ± 0.31	5.04 ± 0.69	2.80 ± 0.38
II	3.69 ± 0.61	3.52	2.35 ± 0.39	5.31 ± 0.88	2.66 ± 0.44
IV	3.57 ± 0.66	3.63	2.27 ± 0.42	5.14 ± 0.95	2.75 ± 0.51

areal superelectron density n_s^{2D} is given by

$$k_B T_{BKT} = \frac{1}{2} \frac{\pi \hbar^2 n_s^{2D}}{m^*}, \quad (2)$$

where m^* is the particle mass which is $2m$ for superconductors. Eq. (2) gives n_s^{2D} , as shown in Table II. In terms of the penetration depth λ , n_s^{2D} satisfies

$$n_s^{2D} = \frac{1}{2} \frac{mc^2}{4\pi e^2} \frac{d}{\lambda^2} = \frac{1}{2} \frac{mc^2}{4\pi e^2} \frac{1}{\lambda_\perp}, \quad (3)$$

where d is the thickness. Beyond the characteristic distance $\lambda_\perp = \lambda^2/d$, proposed by Pearl [27], the logarithmic interaction by the vortices pairs falls off as $1/r$, where r is the distance between the vortices pairs. As shown in Table II, for all the samples, we find λ_\perp has same order magnitude of the sample dimensions (~ 2.5 mm \times 5.0 mm). We therefore conclude that the vortex coupling strength is sufficient to stabilize a BKT state in two-dimensional ReN $_x$ films.

C. $V(I)$ characteristics

To ascertain the absence of incidental long-range order near the BKT transition, data from $V(I)$ measurements are used. The driving mechanisms at the BKT transition require that large currents decouple vortex-antivortex pairs [28]. Then, extra electrical resistance R is generated due to the free vortex. Let n_v be the density of state of free vortex. The extra resistance follows $R = V/I \propto n_v$. It is known that n_v scales with a power law of I . The exponent of I is proportional to superfluid stiffness $J_s(T)$ and T^{-1} , where m is electron mass. Thus, $V(I)$ characteristics around BKT transition is described as

$$V \propto I^\alpha, \alpha = 1 + \frac{\pi J_s(T)}{T}. \quad (4)$$

When the BKT transition occurs ($T = T_{BKT}^\alpha$), $J_s(T_{BKT}^\alpha) = 2T_{BKT}^\alpha/\pi$ and $\alpha = 3$ are expected. The state

with $\alpha = 1$ (*i.e.* $V \propto I$) means normal state. Thereby, we can determine T_{BKT}^α by measuring $V(I)$ curve and estimating the value of α through fitting at various T .

Figures 3(a-c) show the temperature dependence of $V(I)$ curves of samples I, II, and IV, respectively. The interval of the temperature is 0.01 K. The non-linear behavior of the $V(I)$ curves states that the zero resistivity state is attributed not to superconductivity but to the BKT state. We fitted $V(I)$ curves using Eq. (4) to determine α . The fittings are carried out the region where I is larger than the inflection point of $V(I)$. This is to avoid the I region where super- and normal currents mix. Temperature dependence of α is shown in Fig. 3(d-f) of samples I, II, and IV, respectively. $\alpha(T)$ decreases with temperature for samples I, II, and IV except near the inflection point. This reflects the decrease in the superfluid density [7, 26, 29]. The reason why $\alpha(T)$ is not monotonic in sample I and II may be attributed to the phase transition by the remaining superconducting volume. In Fig. 3(e), the dash-dotted line indicates T_{di} of this sample (see also Fig. 1(b)). Below T_{di} , the diamagnetic signal dominates the magnetic response, and the coherency between superelectrons develops below T_{di} . The dip point of $\alpha(T)$ coincides with T_{di} . In $T_{di} < T < T_{BKT}^\alpha$, J_s may have non-monotonic change against the temperature. For sample I, although T_{di} cannot be determined by the magnetization measurement (Fig. 1(a)), the non-monotonic change is likely due to the same reason in sample II. When $T = 3.46$ K, 3.52 K, and 3.63 K, the BKT transition occurs with $\alpha = 3.01 \pm 0.02$, 3.04 ± 0.04 , and 3.00 ± 0.20 in samples I, II, and IV, respectively. This temperature is within the expected range of T_{BKT}^{HN} determined earlier from $\rho(T)$ (see Fig. 2(d-f) and Table II).

D. Magnetoresistance measurement

The BKT transition exist only in the absence of an external magnetic field. If an external magnetic field is applied, the shift in resistivity should be considered as an effective reduction in the vortex-antivortex strength. We investigated H and T dependence of $\rho(T, H)$ to ex-

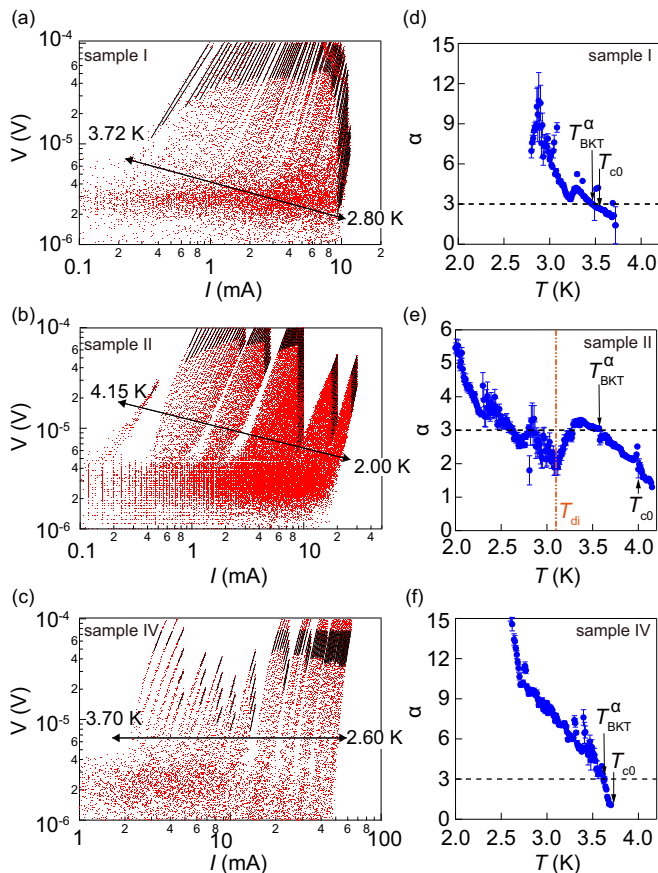


FIG. 3. (a-c) Voltage-current ($V(I)$) characteristics in samples I, II, and IV. The temperature spacing of each $V(I)$ curve is 0.01 K. The measurement range of each $V(I)$ curve is determined to avoid Joule heating effects. The region of fitting $V(I)$ curves to Eq. (4) are shown as full lines in Figs. (a)-(c). (d-f) $\alpha(T)$ estimated by Eq. (4) in samples I, II, and IV. In (e), the dash-dotted line indicates $T_{di} = 3.10$ K, which is defined in Fig. 1(b). The dashed lines in Figs. (d)-(f) mean $\alpha = 3$, where the BKT transition occurs.

amine the temperature dependence of the upper critical field H_{c2} . Strictly speaking, the BKT phase does not have "upper critical field". Nevertheless, $H_{c2} - T$ shows one of the phenomenological proofs of the BKT phase, where H_{c2} is defined by $\rho(T, H_{c2}) = 0$. Thus, we use H_{c2} to compare our results with the previous studies [29–31]. Figures 4(a-c) show the $\rho(T, H)$ mappings. The magnetic field is applied perpendicular to the film surface. The clear transition from the superconducting state (black region) to normal state is observed. This transition corresponds to H_{c2} , and its temperature dependence from the $\rho - H$ curves is shown in Fig. 4(d-f) of samples I, II, and IV, respectively. H_{c2} decreases monotonically with temperature, reflecting the reduction in the vortex-antivortex strength. Below 1.1 K, H_{c2} is linear against the temperature. This is a typical trend for the BKT phase [29–31]. On the other hand, near $T \sim T_{c0}$ in samples I and II, quadratic temperature dependence

with positive curvature is dominant, and the fitting results by $H_{c2} \propto (1 - T/T_{c0})^2$ are shown in the dashed lines. This quadratic behavior is also seen in sample III (see [21]). BKT and Ginzburg-Landau (GL) theories do not give comprehensive representation that H_{c2} is linear in $T \sim 0$ and quadratic in $T \sim T_{c0}$ [32–36]. On the other hand, the papers for multiband superconductivity argue that the power law dependence of H_{c2} in $T \sim T_{c0}$ is attributed to defects and inhomogeneity [37, 38]. In our ReN_x thin films, the two different superconducting phases of ReN and ReN_2 can coexist, and the model for the temperature dependence of H_{c2} in multiband superconductivity is applicable. Additionally, it is consistent with the fact that the quadratic temperature dependence is not observed in sample IV, which has relatively higher crystalline quality.

The intercept of H_{c2} axis ($= H_{c2}(0)$) by the linear fitting between 0.1 K and 1.1 K is estimated to obtain $H_{c2}(0)$, as shown in Table I. According to GL theory, we can discuss inhomogeneity in terms of the coherence length [30]. Using $H_{c2}(0)$, $\xi_{GL}(0) = \sqrt{\Phi_0/2\pi H_{c2}(0)}$, where Φ_0 is flux quantum, can be estimated. In clean limit, $\xi_{GL}(0) \sim \xi_0$ well below T_{c0} . However, one can see $\xi_{GL}(0) \ll \xi_0$ in Table I, implying that the coherence length is dominated by ℓ , and samples I, II, and IV are in dirty limit. Such condition of the samples helps distinguish T_{c0} with T_{BKT} . Nevertheless, excessive inhomogeneity masks the BKT physics, and it can also cause the non-linear $V(I)$ characteristics [7]. Inhomogeneous superconductors have islands with different strength of local superconducting condensates. The finite I can turn the weak superconducting islands into normal ones, resulting in the non-linear $V(I)$ curves at T_{c0} ($\alpha(T_{c0}) > 1$). We take an interface of $\text{LaTiO}_3/\text{SrTiO}_3$ (LTO/STO) as an example to compare with our case [7]. The interface of LTO/STO shows superconductivity, and this conduction is regarded as 2D. Although the interface of LTO/STO is one of the candidates for the BKT transition, the experimental data of the $V(I)$ measurement shows $\alpha(T_{c0}) = 4.5$. This indicates that the BKT analysis by $V(I)$ characteristics is not justified in the LTO/STO because of the excessive inhomogeneity. Notably, the NbN_x thin film shows $\alpha(T_{c0}) = 2.7$. In our case, $\alpha(T_{c0}) = 2.69 \pm 0.03$, 1.83 ± 0.25 and 1.05 ± 0.05 in samples I, II, and IV, respectively. $\alpha(T_{c0})$ decreases with ℓ and $\xi_{GL}(0)$ (see Table I). From the ReN_x samples presented in this investigation, sample IV with $\alpha(T_{c0})$ close to unity highlights advantages of the ReN_x system.

IV. CONCLUSION

We investigated the ReN_x system as a possible materials system to study the BKT phase transition in superconducting systems. Magnetization measurements show a transition from fully diamagnetic thin films towards ReN_x films with a superelectron response. Our analysis of electronic transport parameters concluded that

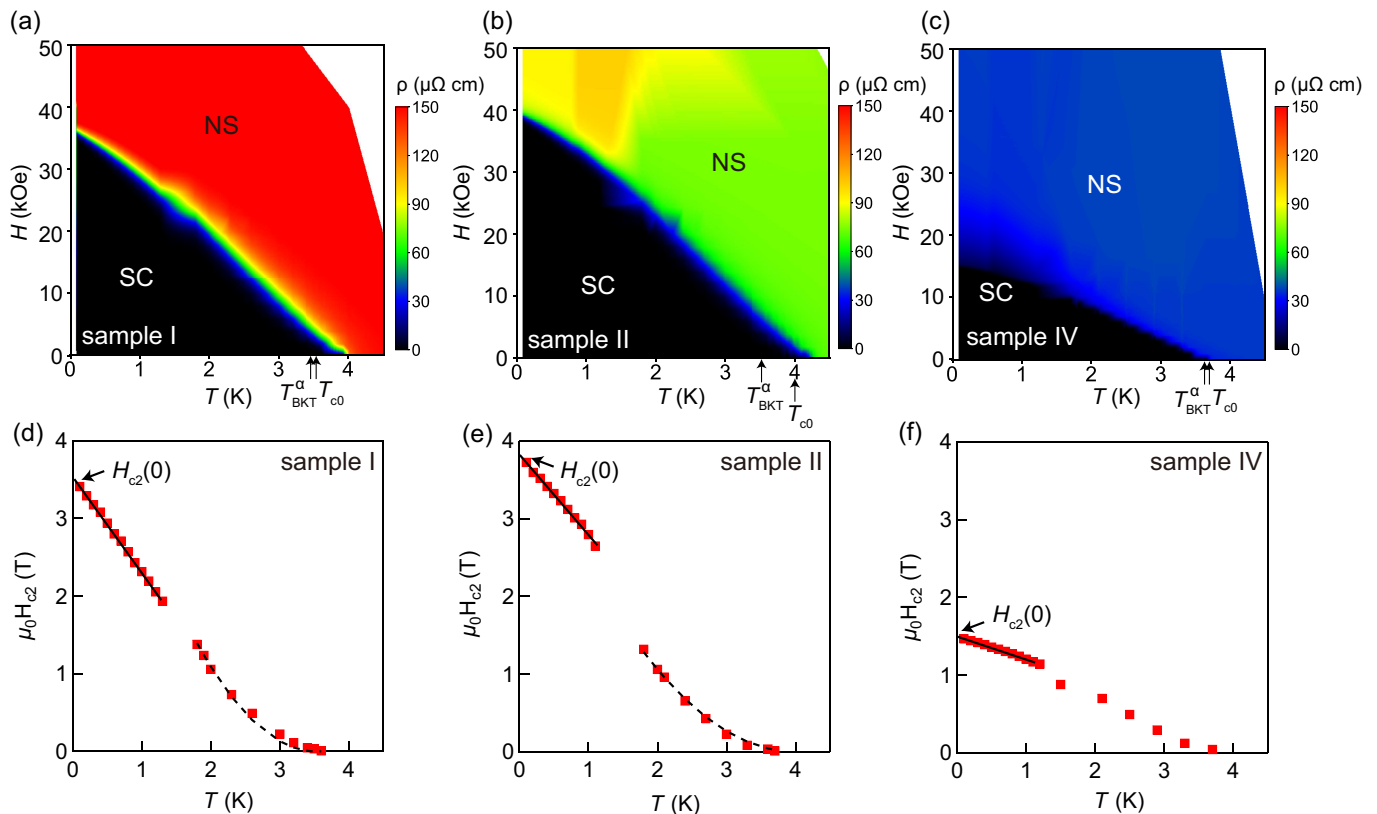


FIG. 4. (a-c) Maps of the resistivity of samples I, II, and IV measured as a function of temperature and external magnetic field in the vicinity of superconductivity. The magnetic field is applied perpendicular to the sample surface. In the black region, $\rho(T, H) = 0$. NS represents the normal state. The color bar indicates the $\rho(T, H)$ variation near the BKT transition. (d-f) Temperature dependence of H_{c2} in samples I, II, and IV. In (d)-(f), solid lines are linear fits. The dashed lines in (d) and (e) are fits to $(H_{c2} \propto (1 - T/T_{c0})^2)$.

the mean free path length can be effectively limited into a regime where $\ell \ll \xi_0$. This approach enabled us to determine critical parameters of the BKT transition in ReN_x . We confirm the hallmarks of the BKT transition in three samples with different superconducting volume by resistivity, $V(I)$, and magnetization measurements. We employed the BMO theory to determine the T_{BKT} temperatures of ReN_x subject to their synthesis parameters. To obtain more precise information about the transition of superfluid stiffness J_s and the mean field critical temperature T_{c0} , the penetration depth measurements and mutual inductance measurements methods are required [4–6]. Nevertheless, the experimental data obtained by the magnetometry and the transport measurements prove that ReN_x is a promising material to investigate BKT physics. Compared with the archetypal system of NbN_x thin films, ReN_x thin films do not need any additional treatment to introduce disorder and inhomogeneity. Furthermore, our ReN_x shows nearly perfect linear relation of $V(I)$ near T_{c0} ($\alpha(T_{c0}) = 1.05$) while $\alpha(T_{c0}) = 2.7$ in NbN_x thin films [7]. Our result suggests that ReN_x thin films can be tuned in a way that allows for sufficient inhomogeneity to instill a topological quantum phase transition like BKT rather than NbN_x .

We conclude that ReN_x is a novel platform for exploring the BKT physics and this work paves the way for potential applications of ReN_x thin films in superconducting devices.

ACKNOWLEDGMENT

The authors thank Takayuki Ikeda for his support in HAADF-STEM, TED and EDX measurements. The authors thank Hiroshi Irie for his inspiring discussion.

REFERENCES

- [1] V. L. Berezinsky, Destruction of long-range order in one-dimensional and two-dimensional systems possessing a continuous symmetry group. ii. quantum systems., *Sov. Phys. JETP* **34**, 610 (1972).
- [2] J. M. Kosterlitz and D. J. Thouless, Ordering, metastability and phase transitions in two-dimensional systems, *J. Phys. C: Solid State Phys.* **6**, 1181 (1973).
- [3] J. M. Kosterlitz, The critical properties of the two-dimensional xy model, *J. Phys. C: Solid State Phys.* **7**, 1046 (1974).

- [4] M. Mondal *et al.*, Role of the vortex-core energy on the Berezinskii-Kosterlitz-Thouless transition in thin films of NbN, *Phys. Rev. Lett.* **107**, 217003 (2011).
- [5] M. Mondal *et al.*, Evolution of Kosterlitz-Thouless-Berezinskii (BKT) transition in ultra-thin NbN films, *J. Phys. Conf. Ser.* **400**, 022078 (2012).
- [6] J. Yong *et al.*, Robustness of the Berezinskii-Kosterlitz-Thouless transition in ultrathin NbN films near the superconductor-insulator transition, *Phys. Rev. B* **87**, 184505 (2013).
- [7] G. Venditti *et al.*, Nonlinear $I - V$ characteristics of two-dimensional superconductors: Berezinskii-Kosterlitz-Thouless physics versus inhomogeneity, *Phys. Rev. B* **100**, 064506 (2019).
- [8] A. Weitzel *et al.*, Sharpness of the Berezinskii-Kosterlitz-Thouless transition in disordered NbN films, *Phys. Rev. Lett.* **131**, 186002 (2023).
- [9] H. Bartolf *et al.*, Current-assisted thermally activated flux liberation in ultrathin nanopatterned NbN superconducting meander structures, *Phys. Rev. B* **81**, 024502 (2010).
- [10] T. I. Baturina *et al.*, Superconducting phase transitions in ultrathin TiN films, *EPL* **97**, 17012 (2012).
- [11] T. D. Nguyen, A. Frydman, and O. Bourgeois, Investigation of specific heat in ultrathin two-dimensional superconducting Pb, *Phys. Rev. B* **101**, 014509 (2020).
- [12] S. P. Chockalingam *et al.*, Superconducting properties and Hall effect of epitaxial NbN thin films, *Phys. Rev. B* **77**, 214503 (2008).
- [13] B. J. van Wees, H. S. J. van der Zant, and J. E. Mooij, Phase transitions of Josephson-tunnel-junction arrays at zero and full frustration, *Phys. Rev. B* **35**, 7291 (1987).
- [14] A. ul. Haq and O. Meyer, Superconducting and electrical properties of rhenium nitride and amorphous rhenium prepared by ion implantation, *J. Low Temp. Phys.* **50**, 123 (1983).
- [15] M. Fuchigami, K. Inumaru, and S. Yamanaka, Interstitial binary nitride ReN_x phases prepared by pulsed laser deposition: Structure and superconductivity dependence on nitrogen stoichiometry, *J. Alloys Compd.* **486**, 621 (2009).
- [16] M. Onodera *et al.*, Rhenium dinitride: Carrier transport in a novel transition metal dinitride layered crystal, *APL Materials* **7**, 101103 (2019).
- [17] A. Friedrich *et al.*, Novel rhenium nitrides, *Phys. Rev. Lett.* **105**, 085504 (2010).
- [18] L. Dubrovinsky *et al.*, Materials synthesis at terapascal static pressures, *Nature* **605**, 274 (2022).
- [19] Z. Zhao *et al.*, Nitrogen concentration driving the hardness of rhenium nitrides, *Sci. Rep.* **4**, 4797 (2014).
- [20] M. R. Beasley, J. E. Mooij, and T. P. Orlando, Possibility of vortex-antivortex pair dissociation in two-dimensional superconductors, *Phys. Rev. Lett.* **42**, 1165 (1979).
- [21] See Supplemental Materials for detailed information about sample preparation and structure determination.
- [22] B. M. Abu-Zied *et al.*, Effect of Pr, Sm, and Tb doping on the morphology, crystallite size, and N_2O decomposition activity of Co_3O_4 nanorods, *J. Nanomater.* **2015**, 580582 (2015).
- [23] H. Liu *et al.*, Strong electronic orbit coupling between cobalt and single-atom praseodymium for boosted nitrous oxide decomposition on Co_3O_4 catalyst, *Environ. Sci. Technol.* **56**, 16325 (2022).
- [24] N. Sclar, Properties of rare-earth nitrides, *J. Appl. Phys.* **35**, 1534 (1964).
- [25] M. R. Koblischka *et al.*, The paramagnetic meissner effect (PME) in metallic superconductors, *Metals* **13**, 1140 (2023).
- [26] B. I. Halperin and D. R. Nelson, Resistive transition in superconducting films, *J. Low Temp. Phys.* **36**, 599 (1979).
- [27] J. Pearl, Current distribution in superconducting films carrying quantized fluxoids, *Appl. Phys. Lett.* **5**, 65 (1964).
- [28] D. R. Nelson and J. M. Kosterlitz, Universal jump in the superfluid density of two-dimensional superfluids, *Phys. Rev. Lett.* **39**, 1201 (1977).
- [29] H. Toyama *et al.*, Two-dimensional superconductivity of Ca-intercalated graphene on SiC: Vital role of the interface between monolayer graphene and the substrate, *ACS Nano* **16**, 3582 (2022).
- [30] M. Yamada, T. Hirahara, and S. Hasegawa, Magnetoresistance measurements of a superconducting surface state of in-induced and Pb-induced structures on Si(111), *Phys. Rev. Lett.* **110**, 237001 (2013).
- [31] A. V. Matetskiy *et al.*, Two-dimensional superconductor with a giant rashba effect: One-atom-layer Tl-Pb compound on Si(111), *Phys. Rev. Lett.* **115**, 147003 (2015).
- [32] N. R. Werthamer, E. Helfand, and P. C. Hohenberg, Temperature and purity dependence of the superconducting critical field, H_{c2} . iii. electron spin and spin-orbit effects, *Phys. Rev.* **147**, 295 (1966).
- [33] K. Maki, The magnetic properties of superconducting alloys. ii, *Phys. Phys. Fiz.* **1**, 127 (1964).
- [34] P.-G. de Gennes, Behavior of dirty superconductors in high magnetic fields, *Phys. Kondens. Mater.* **3**, 79 (1964).
- [35] S. Maekawa, H. Ebisawa, and H. Fukuyama, Upper critical field in two-dimensional superconductors, *J. Phys. Soc. Jpn.* **52**, 1352 (1983).
- [36] R. A. Smith, B. S. Handy, and V. Ambegaokar, Upper critical field in disordered two-dimensional superconductors, *Phys. Rev. B* **61**, 6352 (2000).
- [37] K.-H. Müller *et al.*, The upper critical field in superconducting MgB_2 , *J. Alloys Compd.* **322**, L10 (2001).
- [38] J. M. Edge and A. V. Balatsky, Upper critical field as a probe for multiband superconductivity in bulk and interfacial STO, *J. Supercond. Nov. Magn.* **28**, 2373 (2015).